Optimized growth of compensated ferrimagnetic insulator $Gd_3Fe_5O_{12}$ with a perpendicular magnetic anisotropy

Heng-An Zhou(周恒安), Li Cai(蔡立), Teng Xu(许腾),Yonggang Zhao(赵永刚), and Wanjun Jiang(江万军)
Citation: Chin. Phys. B, 2021, 30 (**9**): 097503. DOI: 10.1088/1674-1056/ac0db0
Journal homepage: http://cpb.iphy.ac.cn; http://iopscience.iop.org/cpb

What follows is a list of articles you may be interested in

Magnetization and magnetic phase diagrams of a spin-1/2 ferrimagnetic diamond chain at low temperature

Tai-Min Cheng(成泰民), Mei-Lin Li(李美霖), Zhi-Rui Cheng(成智睿), Guo-Liang Yu(禹国梁), Shu-Sheng Sun(孙树生), Chong-Yuan Ge(葛崇员), and Xin-Xin Zhang(张新欣)
Chin. Phys. B, 2021, 30 (**5**): 057503. DOI: 10.1088/1674-1056/abd768

Field-induced N\'eel vector bi-reorientation of a ferrimagnetic insulator in the vicinity of compensation temperature

Peng Wang(王鹏), Hui Zhao(赵辉), Zhongzhi Luan(栾仲智), Siyu Xia(夏思宇), Tao Feng(丰韬), and Lifan Zhou(周礼繁)
Chin. Phys. B, 2021, 30 (**2**): 027501. DOI: 10.1088/1674-1056/abbbef

Dyson-Maleev theory of an *X X Z* ferrimagnetic spin chain with single-ion anisotropy

Yu-Ge Chen(陈宇戈), Yin-Xiang Li(李殷翔), Li-Jun Tian(田立君), Bin Chen(陈斌)
Chin. Phys. B, 2018, 27 (**12**): 127501. DOI: 10.1088/1674-1056/27/12/127501

Mn-based permanent magnets

Jinbo Yang(杨金波), Wenyun Yang(杨文云), Zhuyin Shao(邵珠印), Dong Liang(梁栋), Hui Zhao(赵辉), Yuanhua Xia(夏元华), Yunbo Yang(杨云波)
Chin. Phys. B, 2018, 27 (**11**): 117503. DOI: 10.1088/1674-1056/27/11/117503

Random crystal field effect on hysteresis loops and compensation behavior of mixed spin-(1,3/2) Ising system

K Htoutou, Y Benhouria, A Oubelkacem, R Ahl laamara, L B Drissi
Chin. Phys. B, 2017, 26 (**12**): 127501. DOI: 10.1088/1674-1056/26/12/127501

RAPID COMMUNICATION

Optimized growth of compensated ferrimagnetic insulator $Gd_3Fe_5O_{12}$ with a perpendicular magnetic anisotropy*

Heng-An Zhou(周恒安)[1,2], Li Cai(蔡立)[1,2], Teng Xu(许腾)[1,2], Yonggang Zhao(赵永刚)[1,2], and Wanjun Jiang(江万军)[1,2,†]

[1] *State Key Laboratory of Low-Dimensional Quantum Physics and Department of Physics, Tsinghua University, Beijing* 100084, *China*
[2] *Frontier Science Center for Quantum Information, Tsinghua University, Beijing* 100084, *China*

(Received 9 May 2021; revised manuscript received 15 June 2021; accepted manuscript online 23 June 2021)

Compensated ferrimagnetic insulators are particularly interesting for enabling functional spintronic, optical, and microwave devices. Among many different garnets, $Gd_3Fe_5O_{12}$ (GdIG) is a representative compensated ferrimagnetic insulator. In this paper, we will study the evolution of the surface morphology, the magnetic properties, and the magnetization compensation through changing the following parameters: the annealing temperature, the growth temperature, the annealing duration, and the choice of different single crystalline garnet substrates. Our objective is to find the optimized growth condition of the GdIG films, for the purpose of achieving a strong perpendicular magnetic anisotropy (PMA) and a flat surface, together with a small effective damping parameter. Through our experiments, we have found that the surface roughness approaching 0.15 nm can be obtained by choosing the growth temperature around 700 °C, together with an enhanced PMA. We have also found the modulation of magnetic anisotropy by choosing different single crystalline garnet substrates which change the tensile strain to the compressive strain. A measure of the effective magnetic damping parameter ($\alpha_{\rm eff} = 0.04 \pm 0.01$) through a spin pumping experiment in a GdIG/Pt bilayer is also made. Through optimizing the growth dynamics of GdIG films, our results could be useful for synthesizing garnet films with a PMA, which could be beneficial for the future development of ferrimagnetic spintronics.

Keywords: ferrimagnet, perpendicular magnetic anisotropy, ferrite and garnet devices, crystal growth

PACS: 75.50.Gg, 75.30.Gw, 85.70.Ge, 81.10.–h **DOI:** 10.1088/1674-1056/ac0db0

1. Introduction

Rare earth iron garnet (ReIG) of composition $Re_3Fe_5O_{12}$ is one of the most interesting material systems which has continuously attracted attention in the magnetism community[1–4] for storage,[5–9] microwave devices,[10–13] oscillators,[14,15] waveguides,[16–18] magneto-optical isolators,[19–21] spin current generator[22–25] and magnonic devices.[26–30] Very recently, ReIGs with a perpendicular magnetic anisotropy (PMA) appear as a popular material system in the field of spin-orbitronics.[31–35] Particularly, the electrical manipulation of perpendicular magnetization vectors[7,36,37] and the high-speed domain wall (DW) motion,[3,38–40] both enabled by the pure spin currents (in proximity with heavy metal Pt and/or W layers) have been successfully demonstrated. For examples, motion of DW at velocities of 750 m/s[3] and even above 4000 m/s,[40] was recently observed.

Through replacing a nonmagnetic Re element (Y, for example) by the other Re elements with large magnetic moments (Gd,[41,42] Eu,[43] Ho,[44,45] Tb,[46,47] and Dy[48,49] in particular), additional source of magnetism, together with many intriguing properties are introduced.[50–55] Using $Gd_3Fe_5O_{12}$ (GdIG) as an example, it contains three magnetic sublattices,[56,57] the *a*-site Fe^{3+} ions octahedrally coordinated with the surrounding O^{2-} ions, the *d*-site Fe^{3+} ions tetrahedrally coordinated with the O^{2-} ions, and the *c*-site Gd^{3+} ions dodecahedrally coordinated with the O^{2-} ions.[4] The moments of the *a*-site Fe^{3+} ions are antiferromagnetically coupled to the moments of the *d*-site Fe^{3+} ions, which also exhibit a weak ferromagnetic coupling to the moments of the *c*-site Gd^{3+} ions. Through varying temperatures, the net magnetic moments of the Fe^{3+} ions and the Gd^{3+} ions can be fully compensated, manifesting as a magnetization compensation temperature ($T_{\rm M}$).[56–58] On the other hand, due to the slightly different *g* factors of the Fe and Gd elements, the net (spin/orbit) angular moments can also be fully compensated, marked as an angular moment compensation temperature ($T_{\rm A}$). These two characteristic temperatures of the GdIG films, resembling as the equivalent properties of antiferromagnets, have recently brought new exciting opportunities for spintronics.[59,60] The most recently reported ultrafast DW motion[3,38–40] and strong magnon–phonon coupling[61–63] are just a few representative examples. It should be mentioned here that among all ReIGs, GdIG is particularly promising as

*Project supported by the National Key R&D Program of China (Grant Nos. 2017YFA0206200 and 2016YFA0302300), the Basic Science Center Project of the National Natural Science Foundation of China (Grant No. 51788104), the National Natural Science Foundation of China (Grant Nos. 11774194, 11804182, 51831005, and 11811082), Beijing Natural Science Foundation (Grant No. Z190009), and the Beijing Advanced Innovation Center for Future Chip (ICFC).

†Corresponding author. E-mail: jiang_lab@tsinghua.edu.cn

it exhibits the highest (near room temperature) compensation temperature,[56,57] which promises its potential for room temperature ultrafast spintronics.

Note that pulsed laser deposition (PLD) is frequently used for synthesizing high quality garnet films, and complex oxides in general.[43,64,65] The size of sample is however, typically limited to a few millimeters.[66,67] Recently, off-axis magnetron sputtering has been used for growing garnet films with high quality,[68,69] implying that magnetron sputtering is also suitable for growing large area garnet films with high uniformity. However, a systematic investigation of the growth condition and annealing condition on the properties in GdIG is still lacking.

Towards spin-orbitronic applications, GdIG (or ReIG in general) thin films with a PMA at room temperature are demanded. To obtain a GdIG film with a PMA, a tensile strain arising from the lattice mismatch between the GdIG film and the substrate should be carefully examined.[70–72] Since the lattice constant of GdIG is 1.2471 nm,[56–58] we will use single crystalline $Gd_3Sc_2Ga_3O_{12}$ (GSGG) substrate with a lattice constant 1.2554 nm, which could provide a maximum tensile strain that can be beneficial for stabilizing PMA. Note that different growth conditions, including the growth temperature, the annealing temperature/time, the lattice mismatch between substrates and films (and the resulting strain), not only affect the growth dynamics of GdIG films, but also substantially alter the magnetic properties. In this study, we will systematically study the surface morphological, the structural, and the magnetic properties of GdIG films grown under different conditions, aiming for achieving a room temperature PMA and a smooth surface, together with a low effective magnetic damping parameter.

Following this motivation, the evolution of PMA, the surface roughness, and the magnetization compensation of GdIG films will be investigated through changing (a) the annealing temperature, (b) the growth temperature, (c) the substrate pre-annealing temperature, (d) the annealing duration, and (e) the lattice mismatch between different substrates. In the very end, we will quantify (f) the evolution of magnetization compensation temperature as a function of growth parameters and (g) the effective Gilbert damping parameter in the GdIG/Pt bilayer.

2. Results and analyses

GdIG thin films with a fixed (nominal) thickness of 15 nm were deposited on top of various (111)-oriented single crystalline substrates by using a radio-frequency (RF) magnetron sputtering technique, from a commercial target with a nominal composition of $Gd_3Fe_5O_{12}$ by using an ultrahigh vacuum (UHV) sputtering system (AJA-Orion 8). The base pressure of the main chamber is better than 3×10^{-8} Torr. During the deposition, the argon pressure was fixed at 3 mTorr, the deposition rate of GdIG is calibrated to be 0.6 nm/min. An *in-situ* annealing process could be conducted in the sputtering chamber under a mixture of argon and oxygen environment, with an oxygen partial pressure of 20% of 1 mTorr. After annealing, all films were naturally cooled down to room temperature.

A $Gd_3Fe_5O_{12}$ target of nominal composition (99.99%) and various single crystalline substrates used in the present work were commercially available from Kejing, LTD (Hefei, China). X-ray diffraction (XRD) experiments were done by using a Smartlab x-ray diffractometer (Rigaku). Surface morphology was characterized by using a Bruker atomic force microscope (AFM). Magnetometry measurements were done by using a Quantum Design magnetic properties measurement system (MPMS). Transport measurements were done by using a Quantum Design physical properties measurement system (PPMS). All magnetometry, AFM, XRD, and spin pumping experiments were performed at room temperature, unless otherwise specified.

2.1. Annealing effects on the films grown at room temperature

We first synthesized a series of GdIG films of fixed thickness 15 nm on the GSGG (111)-oriented single crystalline substrates at room temperature, which were subsequently annealed *in-situ* in the growth chamber under different annealing temperatures (T_{an}). T_{an} ranges from 400 °C to 800 °C in 100 °C steps, with a fixed duration of 3 hours. Figures 1(a)–1(f) show the corresponding perpendicular magnetization hysteresis loops (M–H_z) of the as-grown GdIG film and the GdIG films annealed at different T_{an}. The as-grown GdIG film does not show any measurable magnetic signal. For $T_{an} \geq 600$ °C, both magnetic signals and square-like hysteresis loops appear, which confirm the presence of PMA of the prepared GdIG films. The evolution of the saturation magnetization (M_s) and the coercivity (H_c), as a function of T_{an}, are summarized in Fig. 1(g). It is clear that M_s starts to increase from $T_{an} = 500$ °C, which reaches a constant value ($M_s = 25$ emu/cc) when $T_{an} \geq 600$ °C. The corresponding H_c increases following the increase of T_{an}.

To correlate the magnetic properties with the film quality, we further studied the surface morphology and the crystal structure of these GdIG films. The evolution of the surface roughness (obtained by performing AFM experiments) as a function of T_{an} is shown in Figs. 2(a)–2(f). A smooth surface of the as-grown GdIG film and the film annealed at 400 °C and 500 °C with a roughness value around 0.15 nm (rms) can be seen. It is also noted that the grain size increases following the increase of T_{an} (≥ 600 °C). Monotonic increases of the height depth (defined as the distance between the highest peak and lowest valley) and roughness (rms) as a function of T_{an} are further shown in Fig. 2(g), which contribute to the enhancement of H_c.

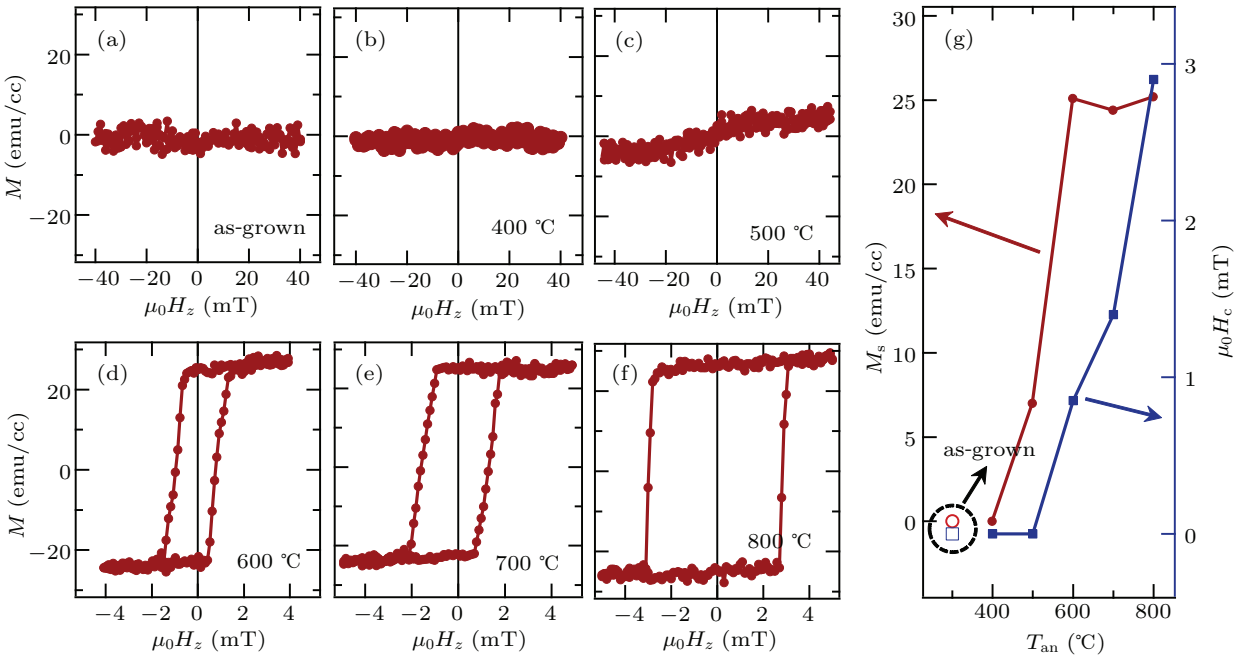

Fig. 1. (a)–(f) The magnetization hysteresis loops (M–H_z) of the as-grown GdIG film and the GdIG films that were annealed at different annealing temperatures (T_{an}). Magnetic fields were applied normal to the film plane (i.e., along the z direction). (g) The evolution of the saturation magnetization (M_s) and coercivity (H_c) as a function of T_{an}.

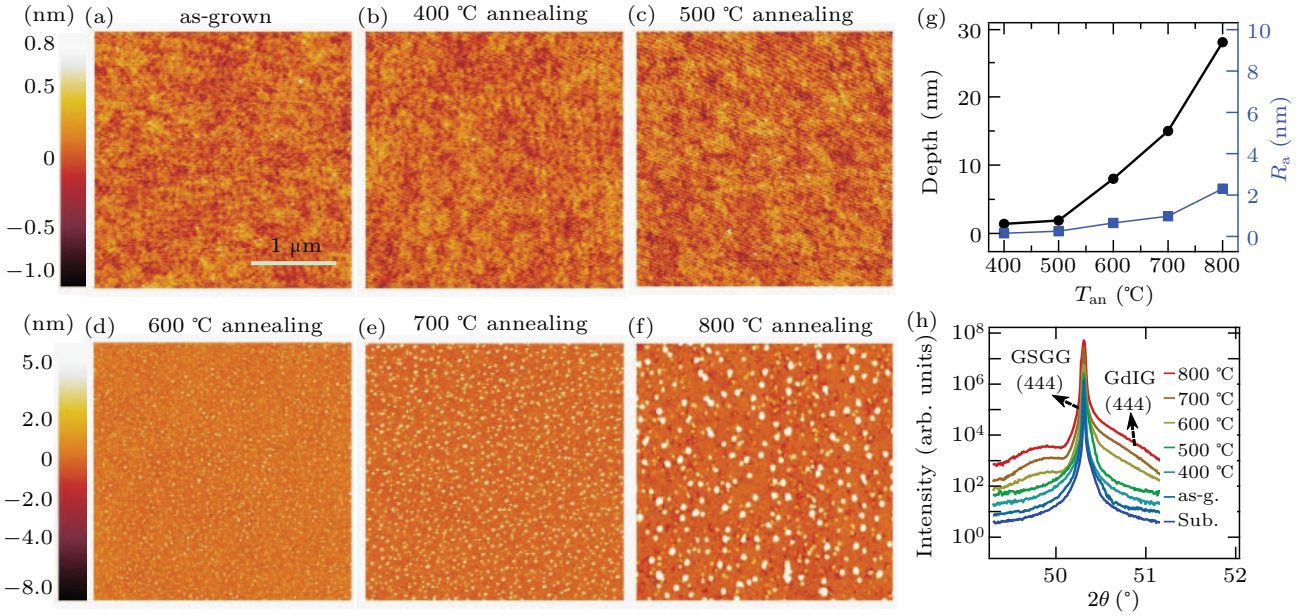

Fig. 2. (a)–(f) A series of AFM images for GdIG films. The increased grain sizes can be found with the increase of annealing temperature T_{an}. (g) The height depth and the surface roughness (rms) as a function of T_{an}. (h) The corresponding XRD spectra of GdIG films, in which diffraction peaks of the GSGG (444) crystal orientation can be seen, together with the GdIG (444) peak when $T_{an} \geq 600$ °C.

It has been previously mentioned that GdIG film with PMA is an ideal platform for spin–orbitronics. For the current-induced spin–orbit torque (SOT) manipulation of the perpendicular magnetization or DW dynamics in the GdIG films, a very thin capping layer of heavy metals (~ 4 nm) with a strong spin–orbit interaction is typically required. For the annealed GdIG films with a PMA, a typical height depth is around 8 nm ($T_{an} = 600$ °C). Thus, a 4 nm heavy metal capping layer cannot ensure a full coverage of GdIG films, which prohibits a further SOT study in these films.

In order to probe the structural properties, we have performed XRD experiments. The x-ray spectra of GdIG films measured around the (444) diffraction peaks of the substrate are shown in Fig. 2(h). It can be seen that the (444) diffraction peaks of the GdIG films are only visible when $T_{an} \geq 600$ °C, which indicate the crystallization of GdIG films. The evolution of the film peak position with respect to the substrate peak position reveals an expected tensile strain from the substrate, which is also consistent with the occurrence of PMA.

2.2. Varying the growth temperature

In the following, we will examine the influence of the growth temperature (T_{gr}) on the film quality. At a relative high growth temperature, atoms with sufficient kinetic energy could easily find the lattice matched location on the substrate, which could naturally give rise to a smoother surface of GdIG film, together with a strong PMA. Note that the growth dynamics by changing growth/annealing temperature (T_{gr}/T_{an}) could be different. In the former case, atoms could move to the corresponding lattice position (during growth) and form a high-quality film. In the latter case, atoms in a grain are not able to move (after growth) between grains during annealing.

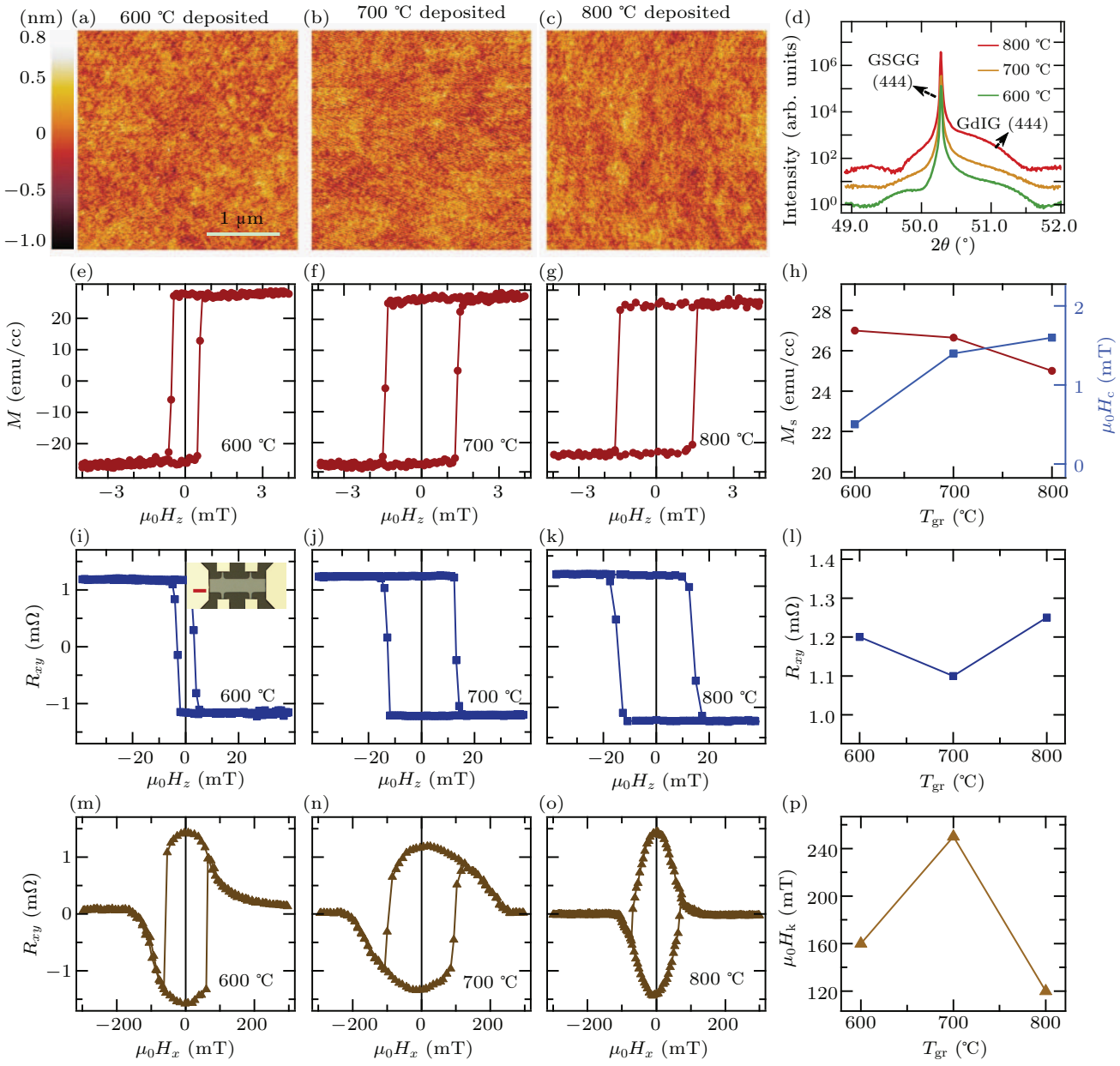

Fig. 3. (a)–(c) The AFM images of GdIG films grown at different temperatures (T_{gr}). (d) The XRD spectra of GdIG films deposited at 600 °C, 700 °C, and 800 °C, respectively. (e)–(g) The corresponding M–H_z loops. (h) The evolution of M_s and H_c as a function of T_{gr}. (i)–(k) The SMR measured in the Hall geometry (R_{xy}^{SMR}) in GdIG/Pt (15 nm/4 nm) bilayers. Shown in the inset is an optical image of Hall bar device. The scale bar is 20 μm. (l) The saturated R_{xy}^{SMR} as function of T_{gr}. (m)–(o) The R_{xy}^{SMR} measured in a planar Hall geometry. (p) The effective field of PMA ($\mu_0 H_k$) as a function of T_{gr}.

Since our previous experiments suggested that GdIG films can crystallize at 600 °C (during the annealing), and meanwhile, exhibit PMA, we will explore the properties of the GdIG films grown at 600 °C, 700 °C, and 800 °C respectively. After deposition, an *in situ* annealing at the corresponding growth temperature for 3 hours was conducted. Figures 3(a)–3(c) are the AFM images of these three samples, in which no visible grains can be seen from the AFM images. The surfaces are very smooth with a roughness (rms) less than 0.19 nm, in stark contrast with the films grown at room temperature (Fig. 2). The corresponding XRD spectra of the GdIG films show (444) diffraction peaks of both substrate and GdIG

film, as shown in Fig. 3(d). Intensity oscillations can also be observed, indicating a high-quality crystallinity and a smooth interface.

We further carried out M–H_z measurement at room temperature, which confirms the presence of PMA in these GdIG films, as shown in Figs. 3(e)–3(g). Both M_s and H_c approach fixed values, when $T_{gr} \geq 700$ °C, as shown in Fig. 3(h). Benefitting from the smooth surfaces, through depositing a 4 nm Pt layer on top of GdIG films, we can detect the magnetic properties electrically by means of spin Hall magnetoresistance (SMR) in the anomalous Hall configuration (R_{xy}^{SMR}).[70,73] Hall devices of width 20 μm and length 120 μm were patterned by using standard photolithography and ion milling techniques. The optical image of the Hall bar device is shown in Fig. 3(i). Figures 3(i)–(k) show R_{xy}^{SMR} acquired in Pt/GdIG bilayer, the evolution of which is similar to the other ReIGs exhibiting PMA, including TmIG/Pt, TbIG/Pt, YIG/Pt, and other bilayers.[7,47,51,74] Note that the H_c values from R_{xy}^{SMR}–H_z measurements are larger than those of M–H_z, which can be attributed to the extra pinning sites introduced during the photolithography process. The amplitude of R_{xy}^{SMR} remains approximately a constant, as shown in Fig. 3(l), which is also consistent with the magnetometry measurement. In order to quantify the effective field of PMA ($\mu_0 H_k$), we have also measured SMR in the planar Hall configuration, as shown in Figs. 3(m)–3(p). It can be seen from Fig. 3(p) that the GdIG film deposited at 700 °C exhibits the strongest PMA.

2.3. Varying the substrate preannealing temperature

It is also known that the substrate quality could affect the magnetic and structural properties of films. We will subsequently examine whether a preannealing procedure on the as-purchased substrate could influence both the film roughness and the strength of PMA. These substrates were preannealed at 500 °C for 0.5 hour before growth in vacuum, as most of adhesive carbides on the substrate will disappear at 500 °C, which could likely give rise to a better film quality. After the preannealing process, we deposited GdIG films at 600 °C and 700 °C, respectively, which were subsequently followed by an *in situ* annealing at the corresponding growth temperature for 3 hours. The AFM images shown in Figs. 4(a) and 4(b) indicate that both films exhibit very smooth surfaces with roughnesses (rms) of 0.17 nm and 0.18 nm, respectively. The magnetic measurements show that the M–H_z loops (Figs. 4(c) and 4(d)) remain the same as those of GdIG films which did not involve a substrate preannealing (Fig. 3). These results indicate that preannealing of the as-purchased substrates is not essential, for which could not improve the quality of the GdIG films.

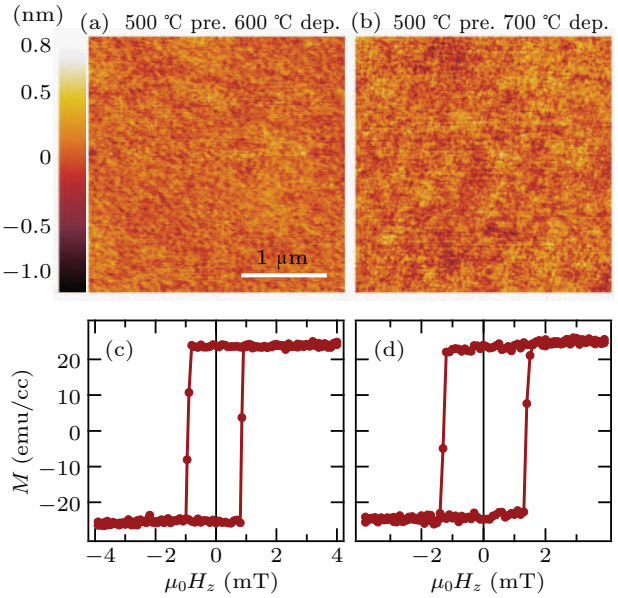

Fig. 4. (a) and (b) AFM images of GdIG films grown on the preannealed substrates. Before the growth of GdIG, GSGG substrates were preannealed at 500 °C for 0.5 hour. The growth temperature of GdIG film is 600 °C and 700 °C, respectively. (c) and (d) M–H_z loops of GdIG films, which remain approximately the same as that of GdIG films grown on the as-purchased substrates (Fig. 3).

2.4. Varying the duration of annealing time

The growth period of GdIG film lasts about 8 hours, we will shorten the growth period by varying the duration of annealing. Note that the growth/annealing temperatures and their raising/falling rates are fixed. In particular, the duration of annealing for enabling smooth surface and PMA of GdIG films will be examined. Four different samples, while all deposited at 700 °C, were *in situ* annealed at 700 °C for 2 hours, 1 hour, 0.5 hour, and 0 hour (immediate cooling down to room temperature in a mixture of argon and oxygen environment), respectively. The surface roughness does not change significantly, as confirmed by the AFM measurements (rms around 0.19 nm), as shown in Figs. 5(a)–5(d). The M–H_z loops show a small decrease of saturation magnetization (from 25 emu/cc to 20 emu/cc), as shown in Figs. 5(e)–5(h). It seems that the GdIG film without subsequent annealing did not crystallize completely during the cooling down. The R_{xy}^{SMR}–H_z measurements from the Hall device made of GdIG/Pt bilayers were also conducted, as shown in Figs. 5(i)–5(p). The influence of the annealing time on the magnetic coercivity H_c obtained from the AHE measurement shows similar evolution to that measured from M–H_z loops. The difference in coercive fields measured from AHE and M–H_z loops can be attributed to the geometry confinement and edge pinning effect introduced during the device fabrication. Figure 5(r) shows the effective field of PMA obtained from PHE measurements, which changes from 245 mT to 140 mT. These results suggest that the longer duration of the annealing, the stronger of the PMA, which saturates when the annealing duration is longer than 2 h.

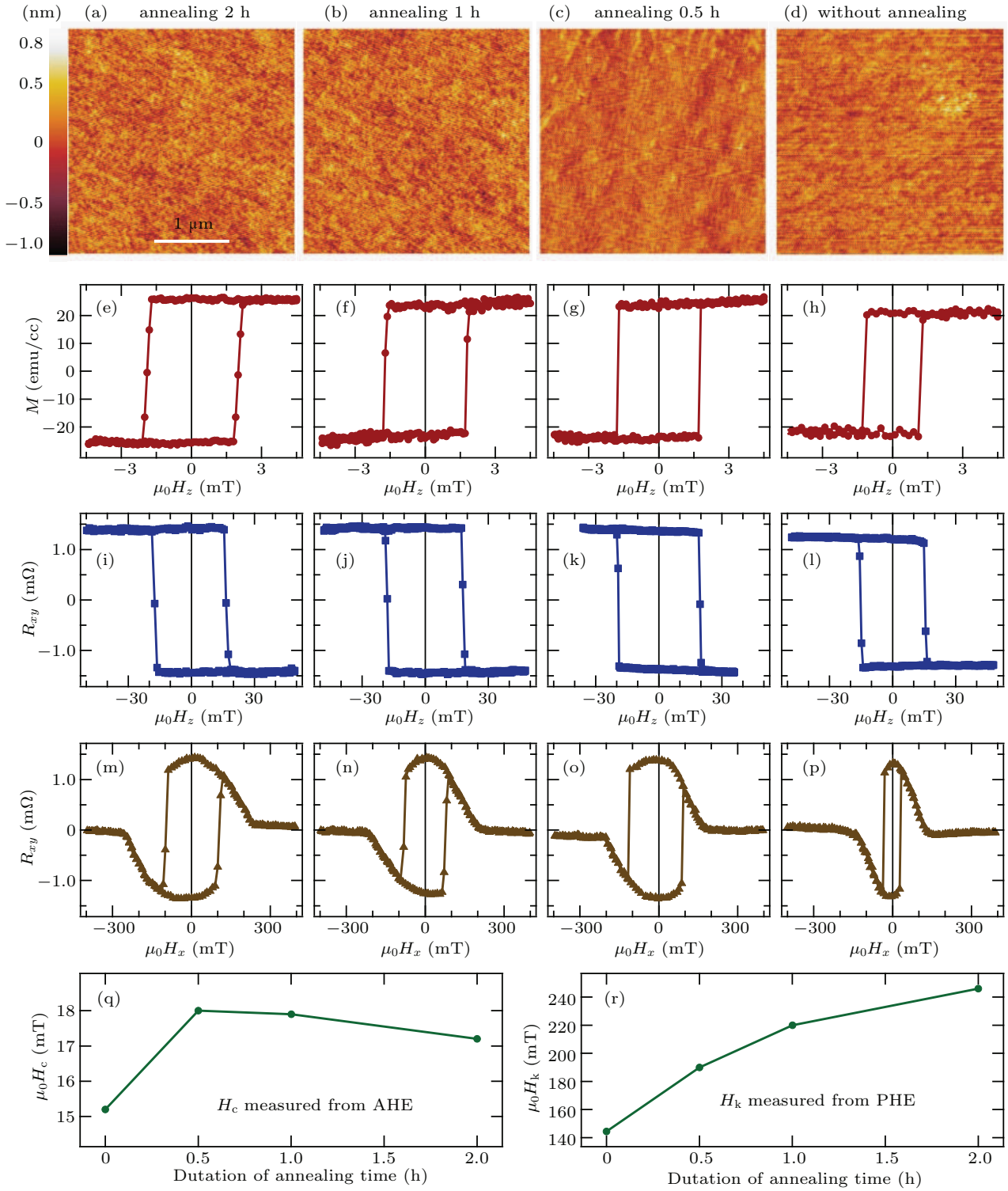

Fig. 5. (a) and (b) The AFM images of GdIG films annealed at 700 °C for 2 hours, 1 hour, 0.2 hour, and 0 hour, respectively. (e)–(h) The M–H_z loops of GdIG films that were being annealed for different durations of time. (i)–(l) and (m)–(p) The corresponding AHE/PHE curves in GdIG/Pt bilayers. (q) and (r) The annealing duration dependent H_c and H_k, obtained from AHE and PHE measurements, respectively.

2.5. Varying substrates with different lattice constants

To elucidate the important role of the strain for stabilizing PMA in GdIG films, we will use different single crystalline garnet substrates with a continuous change of lattice constants. This is made possible by using commercially available garnet substrates, including $Gd_3Sc_2Ga_3O_{12}$ (GSGG), $Gd_{0.63}Y_{2.37}Sc_2Ga_3O_{12}$ (GYSGG), $Gd_{2.6}Ca_{0.4}Ga_{4.1}Mg_{0.25}Zr_{0.65}O_{12}$ (SGGG), and $Y_3Sc_2Ga_3O_5$ (YSGG) (Kejing, LTD). The nominal lattice constants are 1.2554 nm, 1.2507 nm, 1.248 nm, and 1.2426 nm, respectively. These substrates thus provide an ideal platform for examining the evolution of PMA from the tensile strain to the compressive strain. The GdIG films were all deposited at 700 °C, and followed by an *in situ* annealing at 700 °C for

3 hours.

Figures 6(a)–6(d) are the AFM images of GdIG films, all of which exhibit a roughness around 0.17 nm (rms), a result similar to the previous experiments (Figs. 3 and 4). In order to characterize the quality of the GdIG films and calculate the lattice constant of the used substrates, we also performed XRD experiments. Based on the Bragg's law, the lattice constant can be calculated. The positions of (444) peaks lead the lattice constants of GSGG, GYSGG, SGGG, and YSGG to be determined as 1.2552 nm, 1.2506 nm, 1.2481 nm, and 1.2426 nm, respectively. These calculated lattice constants are tabulated in Table 1. Additionally, the Laue fringes on both sides of the (444) peak can be observed from the XRD spectra, as shown in Fig. 6(e).

While both the crystal structure and the surface morphology are very high-quality, the magnetic properties of the GdIG films grown on these different substrates are however, quite different. Figure 6(f) shows the M–H_z loops, which clearly evidence a substrate dependence of magnetic properties. In particular, with a small lattice constant change of 1% between GSGG and YSGG substrates, the magnetic remanence ratio drastically changed from 100% to 5%, as shown in Fig. 6(g). The resultant magnetic anisotropy, as reflected by the shape of M–H_z loops, changes accordingly. These results indicate the important role of lattice mismatch for stabilizing PMA in GdIG films.

Table 1. Detailed material specific parameters of substrates and GdIG films.

	GSGG	GYSGG	SGGG	YSGG	GdIG
Lattice constant (nm)	1.2552	1.2506	1.2481	1.2426	1.2471
2θ (°)	50.313	50.516	50.633	50.868	50.672
Mismatch (%)	0.65	0.28	0.08	–0.3	0

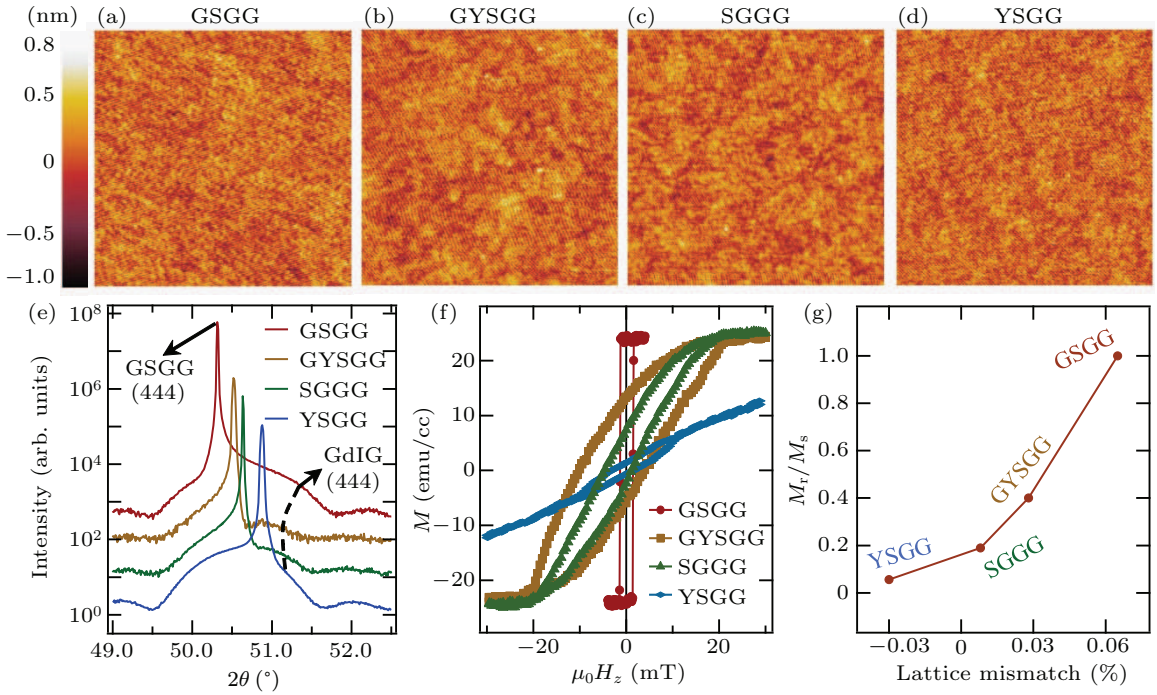

Fig. 6. (a)–(d) The AFM images of GdIG films deposited on top of different single crystalline substrates. (e) The corresponding XRD spectra of GdIG films. (f) The associated M–H_z loops. (g) The lattice mismatch dependent magnetic remanence ratio.

2.6. Evolution of magnetization compensation temperatures

The magnetization compensation temperature (T_M) is an important parameter of compensated ferrimagnets. When the temperature is higher than T_M, the net magnetic moments of the Fe^{3+} ions align with the external magnetic field (the Gd^{3+} ions are against to the external field); when the temperature is lower than T_M, the moments of the Gd^{3+} ions are aligned with the magnetic field (the Fe^{3+} ions are against to the field). In order to rapidly quantify the magnetization compensation temperature, we performed a temperature dependent spin Hall SMR measurement (R_{xy}^{SMR}–T), in the anomalous Hall configuration for GdIG/Pt bilayers.[70,73] Since 4f electrons of the Gd^{3+} ions are in the inner shell, together with the lower Fermi level of the Gd^{3+} ions, the R_{xy}^{SMR}–T measurement is only sensitive to the net magnetization direction of the Fe^{3+} ions,[57,59] which changes sign upon crossing T_M. Thus, a step will appear at T_M in the R_{xy}^{SMR}–T curve, as shown in Fig. 7. At a fixed perpendicular magnetic field ($\mu_0 H_z = +1$ T), a step around 230 K can be clearly seen in each curve. Note that the angular moment compensation temperature (T_A) can be indirectly inferred from the velocity of DW, or directly measured from the angular moment of each sublattices through x-ray circular magnetic dichroism (XMCD).[75,76] It should be mentioned here that the observed T_M in our films is smaller than that of the bulk single crystal ($T_M = 291$ K).[56] Since T_M did not exhibit any depen-

dence on the growth conditions, we tentatively attributed such different values of T_M to the selective sputtering of the GdIG target.

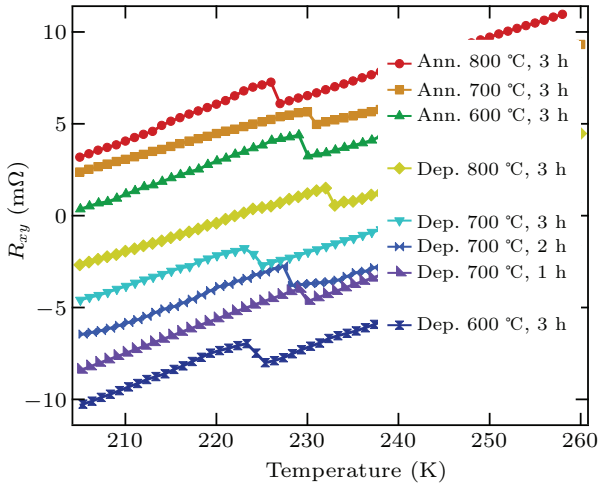

Fig. 7. The R_{xy}^{SMR}–T curves measured in GdIG/Pt bilayer with $H_z = 1$ T. Data is shifted (up and down) for clarity. The sudden jump of R_{xy}^{SMR}–T is identified as T_M.

2.7. The Gilbert damping of GdIG

One of the unique motivations of studying the compensated ferrimagnetic insulator is the absence of conduction electrons, which leads to a low damping parameter that promises their usage in low power consumption spintronics. In the following, we will use a spin pumping technique[25,77] to determine the amplitude of effective damping parameter α_{eff} in a GdIG/Pt bilayer deposited at 700 °C and *in situ* annealed for 2 hours. In this experiment, we fabricated GdIG/Pt microstripes which were integrated with a co-planer waveguide (CPW), as shown in the inset to Fig. 8(a). When a microwave current is fed into the CPW, the accompanied oscillating rf magnetic field drives the precession of magnetization of the GdIG films, which results in the pumping of spin current into the adjacent heavy metal Pt layer. An electrical voltage signal can be subsequently detected, as a result of the inverse spin Hall effect of the Pt layer.

Figure 8(a) shows the spin-pumping voltages measured at different microwave frequencies. During this measurement, the magnetic field H_{IP} was applied in plane with an angle 45° with respect to the GdIG/Pt microstripe. Each spectrum exhibits two symmetrical resonant peaks with an opposite sign, which evolve systematically as a function of the resonant frequency. The resonant linewidth can be obtained by using $V = V_{sp}\Delta H^2/[(H - H_r)^2 + \Delta H^2]$, where V_{sp}, ΔH, and H_r are the amplitudes of spin pumping voltage, linewidth, and resonant field, respectively. Through studying the dependence of the linewidth as a function of the microwave frequency, the effective damping parameter (α_{eff}) can be estimated based on $\Delta H = \Delta H_0 + \alpha_{eff}\omega/\gamma$, as shown in Fig. 8(b). Considering a gyromagnetic ratio $\gamma = 2.8$ GHz/kOe, $\mu_0\Delta H_0 = 8$ mT, $\alpha_{eff} = 0.04 \pm 0.01$ can be obtained. Specifically, the α_{eff} of GdIG/Pt is bigger than that of YIG/Pt (1×10^{-4} to 1×10^{-3}).[25,78] The enhanced damping parameter may originate from the lattice mismatch between GdIG and substrate, or the induced non-collinear spin profile of the Fe^{3+} sublattices due to the presence of the heavy Gd^{3+} ions.[79,80]

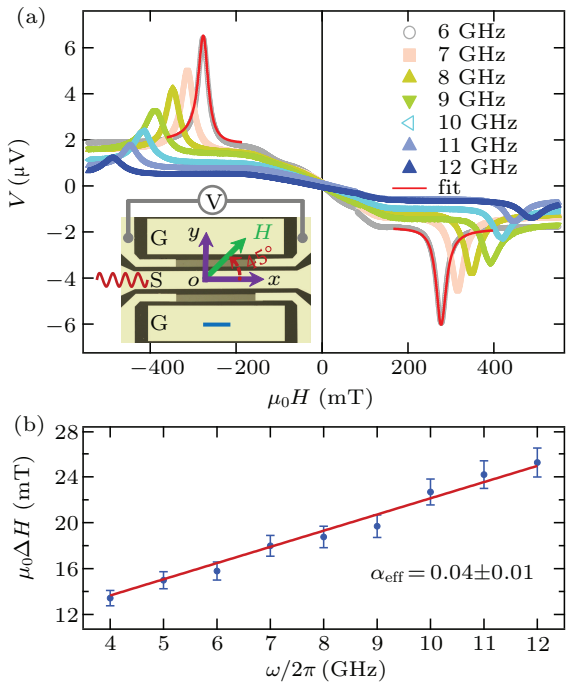

Fig. 8. (a) The resonant spectra measured at different microwave frequencies in the presence of in-pane magnetic fields H_{IP}. Shown in the inset is an optical image of the device, in which GdIG/Pt microstripe is located between CPW. The scar bar is 50 μm. The fitted spin-pumping signal is highlighted in red. (b) The evolution of resonant widths as a function of resonant frequency which can be linearly fitted by using $\Delta H = \Delta H_0 + \alpha_{eff}\omega/\gamma$.

3. Conclusion

In summary, we have systematically studied the surface morphology, the structural properties, and the magnetic properties of compensated ferrimagnetic insulator thin films of composition $Gd_3Fe_5O_{12}$ (GdIG). In particular, the influence of the annealing temperatures/durations, the growth temperatures, and the choice of substrates for ensuring both high-quality growth and the presence of a perpendicular magnetic anisotropy (PMA) were studied. The GdIG films grown at room temperature and annealed at temperature higher than 600 °C exhibit PMA, but a very rough surface. The surface roughness can be substantially improved by changing the growth temperature (≥ 600 °C). And we have found that the strength of PMA reaches maximum when depositing GdIG at 700 °C and following an *in situ* annealing for 2 hours at 700 °C. Furthermore, the effect from the lattice mismatch (and from tensile strain to compressive strain) by choosing different single crystalline ReIG substrates was also examined. In the end, we have also quantified the effective magnetic damping parameter ($\alpha_{eff} = 0.04 \pm 0.01$) through a spin pumping

experiment in a GdIG/Pt microstripe. Through optimizing the growth conditions of GdIG films, our studies could provide useful information for synthesizing similar perpendicularly magnetized ReIG films and their heterostructures, which could be beneficial for developing the efficient compensated ferrimagnetic spintronics.

References

[1] Geller S, Remeika J P, Sherwood R C, Williams H J and Espinosa G P 1965 *Phys. Rev.* **137** A1034

[2] Hansen P, Witter K and Tolksdorf W 1983 *Phys. Rev. B* **27** 4375

[3] Avci C O, Rosenberg E, Caretta L, Büttner F, Mann M, Marcus C, Bono D, Ross C A and Beach G S D 2019 *Nat. Nanotechnol.* **14** 561

[4] Yang Y, Liu T, Bi L and Deng L 2021 *J. Alloys Compd.* **860** 158235

[5] O'Dell T H 1986 *Rep. Prog. Phys.* **49** 589

[6] Moon K W, Kim D H, Yoo S C, Je S G, Chun B S, Kim W, Min B C, Hwang C and Choe S B 2015 *Sci. Rep.* **5** 9166

[7] Avci C O, Quindeau A, Pai C F, Mann M, Caretta L, Tang A S, Onbasli M C, Ross C A and Beach G S D 2017 *Nat. Mater.* **16** 309

[8] Ahmed A S, Lee A J, Bagués N, McCullian B A, Thabt A M A, Perrine A, Wu P K, Rowland J R, Randeria M, Hammel P C, McComb D W and Yang F 2019 *Nano Lett.* **19** 5683

[9] Shao Q, Liu Y, Yu G, Kim S K, Che X, Tang C, He Q L, Tserkovnyak Y, Shi J and Wang K L 2019 *Nat. Electron.* **2** 182

[10] Hansen U H, Demidova V E and Demokritov S O 2009 *Appl. Phys. Lett.* **94** 252502

[11] Collet M, Milly X D, Kelly O D A, Naletov V V, Bernard R, Bortolotti P, Youssef J B, Demidov V E, Demokritov S O, Prieto J L, Munoz M, Cros V, Anane A, Loubens G D and Klein O 2016 *Nat. Commun.* **7** 10377

[12] Zhang D, Song W and Chai G 2017 *J. Phys. D: Appl. Phys.* **50** 205003

[13] Yoshimoto T, Goto T, Shimada K, Iwamoto B, Nakamura Y, Uchida H, Ross C A and Inoue M 2018 *Adv. Electron. Mater.* **4** 1800106

[14] Kiselev S I, Sankey J C, Krivorotov I N, Emley N C, Schoelkopf R J, Buhrman R A and Ralph D C 2003 *Nature* **425** 380

[15] Evelt M, Safranski C, Aldosary M, Demidov V E, Barsukov I, Nosov A P, Rinkevich A B, Sobotkiewich K, Li X, Shi J, Krivorotov I N and Demokritov S O 2018 *Sci. Rep.* **8** 1269

[16] Ghosh S, Keyvavinia S, Roy W V, Mizumoto T, Roelkens G and Baets R 2012 *Opt. Express* **20** 1839

[17] Wang X, Chotorlishvili L, Guo G H and Berakdar J 2018 *J. Appl. Phys.* **124** 073903

[18] Srinivasan K and Stadler B J H 2018 *Opt. Mater. Express* **8** 3307

[19] Dulal P, Block A D, Gage T E, Haldren H A, Sung S Y, Hutchings D C and Stadler B J H 2016 *ACS Photonics* **3** 1818

[20] Mizumoto T, Baets R and Bowers J E 2018 *MRS Bulletin* **43** 419

[21] Deb M, Popova E and Keller N 2019 *Phys. Rev. B* **100** 224410

[22] Uchida K, Xiao J, Adachi H, Ohe J, Takahashi S, Ieda J, Ota T, Kajiwara Y, Umezawa H, Kawai H, Bauer G E W, Maekawa S and Saitoh E 2010 *Nat. Mater.* **9** 894

[23] Heinrich B, Burrowes C, Montoya E, Kardasz B, Girt E, Song Y Y, Sun Y and Wu M 2011 *Phys. Rev. Lett.* **107** 066604

[24] Uchida K, Nonaka T, Kikkawa T, Kajiwara Y and Saitoh E 2013 *Phys. Rev. B* **87** 104412

[25] Wang H L, Du C H, Pu Y, Adur R, Hammel P C and Yang F Y 2014 *Phys. Rev. Lett.* **112** 197201

[26] Chumak A V, Vasyuchka V I, Serga A A and Hillebrands B 2015 *Nat. Phys.* **11** 453

[27] Cornelissen L J, Liu J, Duine R A, Youssef J B and van Wees B J 2015 *Nat. Phys.* **11** 1022

[28] Qin H, Both G J, Hämäläinen J, Yao L and van Dijken S 2018 *Nat. Commun.* **9** 5445

[29] Chen J, Wang C, Liu C, Tu S, Bi L and Yu H 2019 *Appl. Phys. Lett.* **114** 212401

[30] Vilela G L S, Abrao J E, Santos E, Yao Y, Mendes J B S, Rodríguez-Suárez R L, Rezende S M, Han W, Azevedo A and Moodera J S 2020 *Appl. Phys. Lett.* **117** 122412

[31] Quindeau A, Avci C O, Liu W, Sun C, Mann M, Tang A S, Onbasli M C, Bono D, Voyles P M, Xu Y, Robinson J, Beach G S D and Ross C A 2017 *Adv. Electron. Mater.* **3** 1600376

[32] Rosenberg E R, Beran L, Avci C O, Zeledon C, Song B, Gonzalez-Fuentes C, Mendil J, Gambardella P, Veis M, Garcia C, Beach G S D and Ross C A 2018 *Phys. Rev. Mater.* **2** 94405

[33] Ding S, Ross A, Lebrun R, Becker S, Lee K, Boventer I, Das S, Kurokawa Y, Gupta S, Yang J, Jakob G and Kläui M 2019 *Phys. Rev. B* **100** 100406

[34] Ryu J, Lee S, Lee K J and Park B G 2020 *Adv. Mater.* **32** 1907148

[35] Li G, Bai H, Su J, Zhu Z Z, Zhang Y and Cai J W 2019 *APL Mater.* **7** 041104

[36] Shao Q, Grutter A, Liu Y, Yu G, Yang C Y, Gilbert D A, Arenholz E, Shafer P, Che X, Tang C, Aldosary M, Navabi A, He Q L, Kirby B J, Shi J and Wang K L 2019 *Phys. Rev. B* **99** 104401

[37] Ding J, Liu C, Zhang Y, Erugu U, Quan Z, Yu R, McCollum E, Mo S, Yang S, Ding H, Xu X, Tang J, Yang X and Wu M 2020 *Phys. Rev. Appl.* **14** 014017

[38] Avci C O, Rosenberg E, Baumgartner M, Beran L, Quindeau A, Gambardella P, Ross C A and Beach G S D 2017 *Appl. Phys. Lett.* **111** 072406

[39] Vélez S, Schaab J, Wörnle M S, Müller M, Gradauskaite E, Welter P, Gutgsell C, Nistor C, Degen C L, Trassin M, Fiebig M and Gambardella P 2019 *Nat. Commun.* **10** 4750

[40] Caretta L, Oh S H, Fakhrul T, Lee D K, Lee B H, Kim S K, Ross C A, Lee K J and Beach G S D 2020 *Science* **370** 1438

[41] Kuila M, Hussain Z and Reddy V R 2019 *J. Magn. Magn. Mater.* **473** 458

[42] Bayaraa T, Xu C, Campbell D and Bellaiche L 2019 *Phys. Rev. B* **100** 214412

[43] Ortiz V H, Aldosary M, Li J, Xu Y, Lohmann M I, Sellappan P, Kodera Y, Garay J E and Shi J 2018 *APL Mater.* **6** 121113

[44] Kalashnikova A M, Pavlov V V, Kimel A V, Kirilyuk A, Rasing T and Pisarev R V 2012 *Low Temp. Phys.* **38** 863

[45] Ghanathe M, Kumar A, da Silva I and Yusuf S M 2021 *J. Magn. Magn. Mater.* **523** 167632

[46] Srinivasan K, Radu C, Bilardello D, Solheid P and Stadler B J H 2020 *Adv. Funct. Mater.* **30** 2000409

[47] Chen H, Cheng D, Yang H, Wang D, Zhou S, Shi Z and Qiu X 2020 *Appl. Phys. Lett.* **116** 112401

[48] Zhang Y, Du Q, Wang C, Yan W, Deng L, Hu J, Ross C A and Bi L 2019 *APL Mater.* **7** 081119

[49] Bauer J J, Rosenberg E R, Kundu S, Mkhoyan K A, Quarterman P, Grutter A J, Kirby B J, Borchers J A and Ross C A 2019 *Adv. Electron. Mater.* **6** 1900820

[50] Pamyatnykh L A, Agafonov L Y, Belskii I E and Balymov K G 2017 *IEEE Trans. Magn.* **53** 1

[51] Liu Y K, Wong H F, Lam K K, Chan K H, Mak C L and Leung C W 2018 *J. Magn. Magn. Mater.* **468** 235

[52] Boutaba A, Lahoubi M, Varazashvili V and Pu S 2019 *J. Magn. Magn. Mater.* **476** 551

[53] Strohm C, Linden P V D, Mathon O and Pascarelli S 2019 *Phys. Rev. Lett.* **122** 127204

[54] Kudasov Y B and Kozabaranov R V 2019 *Journal of Physics: Conference Series* **1389** 012109

[55] Liensberger L, Kamra A, Maier-Flaig H, Geprags S, Erb A, Goennenwein S T B, Gross R, Belzig W, Huebl H and Weiler M 2019 *Phys. Rev. Lett.* **123** 117204

[56] Uemura M, Yamagishi T, Ebisu S, Chikazawa S and Nagata S 2008 *Philos Mag (Abingdon)* **88** 209

[57] Dong B W, Cramer J, Ganzhorn K, Yuan H Y, Guo E J, Goennenwein S T B and Kläui M 2018 *J. Phys. Condens. Matter* **30** 035802

[58] Zanjani S and Onbaşlı M C 2020 *J. Magn. Magn. Mater.* **499** 166108

[59] Finley J and Liu L 2020 *Appl. Phys. Lett.* **116** 110501

[60] Zhou H A, Xu T, Bai H and Jiang W 2021 *J. Phys. Soc. Jpn.* **90** 081006

[61] Man H, Shi Z, Xu G, Xu Y, Chen X, Sullivan S, Zhou J, Xia K, Shi J and Dai P 2017 *Phys. Rev. B* **96** 100406

[62] Wang L W, Xie L S, Xu P X and Xia K 2020 *Phys. Rev. B* **101** 165137

[63] Bozhko D A, Vasyuchka V I, Chumak A V and Serga A A 2020 *Low Temp. Phys.* **46** 383

[64] Soumah L, Beaulieu N, Qassym L, Carrétéro C, Jacquet E, Lebourgeois R, Youssef J B, Bortolotti P, Cros V and Anane A 2018 *Nat. Commun.* **9** 3355
[65] Mendil J, Trassin M, Bu Q, Schaab J, Baumgartner M, Murer C, Dao P T, Vijayakumar J, Bracher D, Bouillet C, Vaz C A F, Fiebig M and Gambardella P 2019 *Phys. Rev. Mater.* **3** 034403
[66] Chrisey D B and Hublerm G K 1994 *Pulsed Laser Deposition of Thin Films* (Wiley-Interscience)
[67] Kuppusami P and Raghunathan V S 2006 *Surf. Eng.* **22** 81
[68] Wu C N, Tseng C C, Lin K Y, Cheng C K, Yeh S L, Fanchiang Y T, Hong M and Kwo J 2018 *AIP Adv.* **8** 055904
[69] Chen C C, Chen K H M, Fanchiang Y T, Tseng C C, Yang S R, Wu C N, Guo M X, Cheng C K, Huang S W, Lin K Y, Wu C T, Hong M and Kwo J 2019 *Appl. Phys. Lett.* **114** 031601
[70] Tang C, Sellappan P, Liu Y, Xu Y, Garay J E and Shi J 2016 *Phys. Rev. B* **94** 140403
[71] Wu C N, Tseng C C, Fanchiang Y T, Cheng C K, Lin K Y, Yeh S L, Yang S R, Wu C T, Liu T, Wu M, Hong M and Kwo J 2018 *Sci. Rep.* **8** 11087
[72] Vilela G, Chi H, Stephen G, Settens C, Zhou P, Ou Y, Suri D, Heiman D and Moodera J S 2020 *J. Appl. Phys.* **127** 115302
[73] Chen Y T, Takahashi S, Nakayama H, Althammer M, Goennenwein S T B, Saitoh E and Bauer G E W 2013 *Phys. Rev. B* **87** 144411
[74] Liu Q B, Meng K K, Xu Z D, Zhu T, Xu X G, Miao J and Jiang Y 2020 *Phys. Rev. B* **101** 174431
[75] Vasili H B, Casals B, Cichelero R, Macià F, Geshev J, Gargiani P, Valvidares M, Herrero-Martin J, Pellegrin E, Fontcuberta J and Herranz G 2017 *Phys. Rev. B* **96** 014433
[76] Siddiqui S A, Han J, Finley J T, Ross C A and Liu L 2018 *Phys. Rev. Lett.* **121** 057701
[77] Zhou H, Fan X, Ma L, Zhang Q, Cui L, Zhou S, Gui Y S, Hu C M and Xue D 2016 *Phys. Rev. B* **94** 134421
[78] Dubs C, Surzhenko O, Thomas R, Osten J, Schneider T, Lenz K, Grenzer J, Hübner R and Wendler E 2020 *Phys. Rev. Mater.* **4** 024416
[79] Kehlberger A, Richter K, Onbasli M C, Jakob G, Kim D H, Goto T, Ross C A, Götz G, Reiss G, Kuschel T and Kläui M 2015 *Phys. Rev. Appl.* **4** 014008
[80] Crossley S, Quindeau A, Swartz A G, Rosenberg E R, Beran L, Avci C O, Hikita Y, Ross C A and Hwang H Y 2019 *Appl. Phys. Lett.* **115** 172402